Study of phase diagram and superconducting states in $LaFeAsO_{1-x}H_x$ based on the multiorbital extended Hubbard model

Y. Yamakawa[1], S. Onari[2], H. Kontani[1], N. Fujiwara[3], S. Iimura[4], and H. Hosono[4]
[1] *Department of Physics, Nagoya University, Furo-cho, Nagoya 464-8602, Japan.*
[2] *Department of Applied Physics, Nagoya University, Furo-cho, Nagoya 464-8602, Japan.*
[3] *Graduate School of Human and Environmental Studies, Kyoto University, Yoshida-Nihonmatsu-cho, Sakyo-ku, Kyoto 606-8501, Japan.*
[4] *Materials and Structures Laboratory, Tokyo Institute of Technology, 4259 Nagatsuta-cho, Midori-ku, Yokohama 226-8503, Japan.*
(Dated: April 16, 2013)

To understand the recently established unique magnetic and superconducting phase diagram of $LaFeAsO_{1-x}H_x$, we analyze the realistic multiorbital tight-binding model for $x = 0 \sim 0.4$ beyond the rigid band approximation. Both the spin and orbital susceptibilities are calculated in the presence of the Coulomb and charge quadrupole interactions. It is found that both orbital and spin fluctuations strongly develop at both $x \sim 0$ and 0.4, due to the strong violation of the rigid band picture in $LaFeAsO_{1-x}H_x$. Based on this result, we discuss the experimental phase diagram, especially the double-dome superconducting phase. Moreover, we show that the quadrupole interaction is effectively produced by the vertex correction due to Coulomb interaction, resulting in the mutual development of spin and orbital fluctuations.

PACS numbers: 74.70.Xa, 74.20.-z, 74.25.Dw

Since the discovery of high-T_c superconductivity in Fe-based superconductors [1], its pairing mechanism has been studied very intensively. In unconventional superconductors, the phase-diagram in the normal state gives us very important hints to understand the mechanism of superconductivity. In many heavy fermion superconductors, for example, the superconducting (SC) phase is next to the magnetic ordered phase, indicating the occurrence of spin-fluctuation mediated superconductivity. In Fe-based superconductors, in contrast, the ferro-orbital order occurs in the orthorhombic phase [2, 3], and the structure or orbital instabilities are realized in the normal state [4, 5], in addition to the magnetic instability. Based on this fact, both the spin-fluctuation mediated $s_{\pm}$-wave state [6–9] and the orbital-fluctuation mediated s_{++}-wave state [10–12] have been discussed. The former (latter) SC gap with (without) sign reversal is induced by repulsive (attractive) interaction between electron-like and hole-like Fermi surfaces (FSs).

Recently, very unique phase diagram of H-doped LaFeAsO, $LaFeAsO_{1-x}H_x$, is determined in Ref. [13]: The structure and magnetic transitions in mother compound are replaced with the SC phase at $x \sim 0.03$, and interesting double-dome structure of T_c is obtained between $x = 0.03$ and $\lesssim 0.5$. The maximum T_c of the first (second) dome is about 25 K (40 K) at $x \sim 0.1$ ($x \sim 0.35$). For $x > 0.4$, recent NMR measurement [14] detected the incommensurate magnetic order, in addition to the highly anisotropic electric field gradient that indicates the occurrence of the non-magnetic orbital order.

In $LaFeAsO_{1-x}H_x$, the electron filling per Fe is $n = 6+x$ since each H-dopant becomes H^- ion, and therefore the electronic states are expected to be similar to those of $LaFeAsO_{1-x}F_x$ [13]. Based on this fact, the band structure and FSs for $x = 0 \sim 0.4$ had been derived from the local-density-approximation (LDA) band calculation using the virtual crystal approximation in Ref. [13]. It is found that the rigid band picture is no more valid, since the band structure is strongly modified with increasing F-doping. The derived realistic band structure now enables us to perform quantitative theoretical study of the pairing mechanism of 1111 systems.

In this paper, we study the electronic and SC states in $LaFeAsO_{1-x}H_x$ for $x = 0 \sim 0.4$, by constructing the realistic multiorbital models beyond the rigid band approximation. Using the random-phase-approximation (RPA), both the spin and orbital susceptibilities are calculated in the presence of the Coulomb interaction U and charge quadrupole interaction g. Assuming monotonic x-dependencies of these interactions, strong spin and orbital fluctuations are obtained for both $x \sim 0$ and $x \sim 0.4$. Based on this result, the origin of the double-dome structure of T_c in $LaFeAsO_{1-x}H_x$ is discussed, by applying both the orbital-fluctuation mediated s_{++}-wave scenario and spin-fluctuation mediated $s_{\pm}$-wave one. We discuss that g is effectively induced by the vertex correction (VC) of the Coulomb interaction beyond the RPA.

In $LaFeAsO_{1-x}F_x$, the spin fluctuations observed by NMR and neutron inelastic scattering are very small in slightly over-doped compounds ($x \sim 0.08$). In the over-doped compound with $x = 0.14$, T_c increases from 20K to 43K by applying 3.7GPa, irrespective that $1/T_1T$ remains very small independently of the pressure [15]. These facts indicate the weak correlation between T_c and spin fluctuations. Moreover, impurity effect on T_c is very small in both 1111 [16, 17] and 122 [18, 19] compounds, indicating the realization of the s_{++}-wave state [20, 21]. Unfortunately, these experiments on $LaFeAsO_{1-x}H_x$ have not been performed yet.

First, we perform the LDA band calculation for

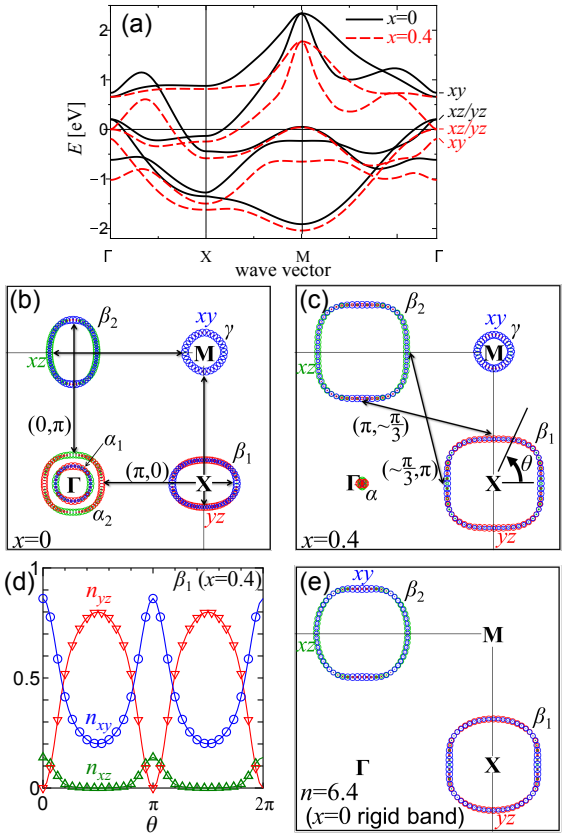

FIG. 1: (Color online) (a) Band structures for $x = 0$ (solid line) and $x = 0.4$ (dashed line) in the present model. (b) FSs for $x = 0$ and (c) FSs for $x = 0.4$. The weights of xz-, yz- and xy-orbital on the Fermi surfaces are represented by diameter of green-, red-, and blue-circles, respectively. (d) Weight of orbitals on the Fermi surface around X point for $x = 0.4$ as a function of azimuthal angle θ. (e) FSs for $n = 6.4$ given by the rigid band model for LaFeAsO.

$LaFeAsO_{1-x}F_x$ for $x = 0 \sim 0.4$ using WIEN2K code with virtual crystal approximation, where the oxygen sites are substituted for virtual atoms with a fractional nuclear charge. Since H^{-1} ion acts as F^{-1} ion, the electronic states of $LaFeAsO_{1-x}H_x$ are expected to be similar to those of $LaFeAsO_{1-x}F_x$ [13]. Next, we derive the two-dimensional five-orbital tight-binding models for each x using WANNIER90 code and WIEN2WANNIER interface [22]: $\hat{H}^0 = \sum_{\boldsymbol{k}lm\sigma} h^{l,m}_{\boldsymbol{k}} c^\dagger_{\boldsymbol{k}l\sigma} c_{\boldsymbol{k}m\sigma}$, where $l, m = 1-5$ represent the d orbitals with the order $3z^2 - r^2$, xz, yz, xy, and $x^2 - y^2$: Here, we set x and y axes parallel to the nearest Fe-Fe bonds.

Figure 1 (a) shows the band structures of $LaFeAsO_{1-x}F_x$ in the present model. It is obvious that band structure for $x = 0.4$ cannot be reproduced by the rigid band shift from that for $x = 0$. The corresponding FSs are shown in Fig. 1 (b) and (c). Here, β_1 and β_2 are the electron-pockets, and α_1, α_2 and γ are the hole-pockets, both of which are composed of the three xz-, yz- and xy-orbitals: The orbital character of the electron-pocket for $x = 0.4$ is shown in Fig. 1 (d). In the case of $x = 0$, the electron-hole (e-h) FS nesting with the nesting vector $\boldsymbol{Q} = (\pi, 0), (0, \pi)$ is the most important. On the other hand, in the case of $x = 0.4$, electron-electron (e-e) FS nesting $\boldsymbol{Q} \sim (\pi, \pi/3), (\pi/3, \pi)$ is more important since the hole pockets become very small. In both $x = 0$ and $x = 0.4$, both the intra-orbital nesting and inter-orbital nesting (between xz/yz and xy) are important. Then, the former (latter) nesting gives rise to the strong spin (orbital) fluctuations, as discussed in Ref. [10].

Fig. 1 (e) shows the FSs for $n = 6.4$ given by the model parameters for $x = 0$ (LaFeAsO). In this "rigid-band approximation", the hole pockets disappear, and the e-e FS nesting is worse since the shape of the electron-pockets are more rounded.

Next, we explain the interaction term. We introduce both the Coulomb interaction (U, U', J, J') and quadrupole interaction (g). The latter interaction is

$$V_{\rm quad} = -g(\omega_l) \sum_i^{\rm site} \left(\hat{O}^i_{xz} \cdot \hat{O}^i_{xz} + \hat{O}^i_{yz} \cdot \hat{O}^i_{yz} + \hat{O}^i_{xy} \cdot \hat{O}^i_{xy} \right), \tag{1}$$

where $g(\omega_l) = g \cdot \omega_c^2/(\omega_l^2 + \omega_c^2)$: $g = g(0)$ is the quadrupole interaction at $\omega_l = 2l\pi T = 0$, and ω_c is the cutoff energy. $\hat{O}_\Gamma$ is the quadrupole operator [10], which has many non-zero off-diagonal elements. By introducing small g ($\sim$ 0.2eV), strong $O_{xz,yz}$-type antiferro-quadrupole fluctuations are caused by the good inter-orbital nesting, as explained in Ref. [10].

Now, we perform the RPA for the present model at $T = 0.02$eV, by assuming that $J = J'$ and $U = U' + 2J$, and fix the ratio $J/U = 1/6$. We use $64 \times 64\boldsymbol{k}$ meshes and 512 Matsubara frequencies. We set the unit of energy as eV hereafter. The spin (orbital) susceptibility in the RPA is given by

$$\hat{\chi}^{\rm s(c)}(q) = \hat{\chi}^0(q) \left[\hat{1} - \hat{\Gamma}^{\rm s(c)}(\omega_l) \hat{\chi}^0(q) \right]^{-1}, \tag{2}$$

where $q = (\boldsymbol{q}, \omega_l)$, and $\hat{\Gamma}^{s(c)}$ is the interaction matrix for the spin (charge) channel composed of U, U', J, J' and $g(\omega_l)$ [10]. $\hat{\chi}^0(q) = -\frac{T}{N} \sum_k G_{lm}(k+q) G_{m'l'}(k)$ is the irreducible susceptibility, where $\hat{G}(k) = [i\epsilon_n + \mu - \hat{h}_{\boldsymbol{k}}]^{-1}$ is the bare Green function, and $\epsilon_n = (2n+1)\pi T$.

The magnetic (orbital) order is realized when the spin (charge) Stoner factor $\alpha_{\rm s(c)}$, which is the maximum eigenvalue of $\hat{\Gamma}^{\rm s(c)} \hat{\chi}^{(0)}(\boldsymbol{q}, 0)$, is unity. In the RPA, the enhancement of $\hat{\chi}^{\rm s}$ is mainly caused by the intra-orbital Coulomb interaction U, using the "intra-orbital nesting" of the FSs. On the other hand, the enhancement of $\hat{\chi}^{\rm c}$ in the present model is caused by the quadrupole interaction in Eq. (1), utilizing the "inter-orbital nesting" of the FSs.

Now, we study the development of the spin susceptibility by U, by putting $g = 0$. Figure 2 shows the total spin susceptibility $\chi^s(\boldsymbol{q}, \omega = 0) \equiv \sum_{l,m} \chi^s_{ll,mm}(\boldsymbol{q})$

for $x = 0, 0.14, 0.24, 0.4$, by choosing the U to realize $\alpha_s = 0.98$. For (a) $x = 0$, $\chi^s(\boldsymbol{q})$ has commensurate peaks at $\boldsymbol{q} = (\pi, 0)$ and $(0, \pi)$ due to the e-h FS nesting. These peaks change to incommensurate for (b) $x = 0.14$, reflecting the size imbalance between electron- and hole-pockets. As increasing the doping further, the e-e FS nesting and e-h FS nesting become comparable. Because of the fact, $\chi^s(\boldsymbol{q})$ for (c) $x = 0.24$ shows the double-peak structure. For (d) $x = 0.4$, $\chi^s(\boldsymbol{q})$ shows the incommensurate peak structure due to the e-e FS nesting only.

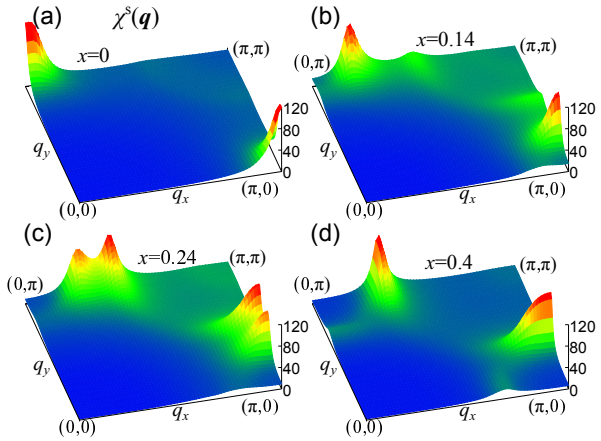

FIG. 2: (Color online) $\boldsymbol{q}$-dependence of $\chi^s(\boldsymbol{q})$ with $\alpha_s = 0.98$ for (a) $x = 0$, (b) $x = 0.14$, (c) $x = 0.24$ and (d) $x = 0.4$.

Figure 3 (a) shows the x-dependence of U_c, which is the critical value of U for the spin order given by the condition $\alpha_s = 1$. We stress that U_c in the present model is much smaller than that in the rigid band model, reflecting the good e-h (e-e) FS nesting for $x < 0.24$ ($x > 0.24$) in the present model. Moreover, U_c takes the maximum value at $x \approx 0.1$, and monotonically decreases by departing from $x \approx 0.1$. For this reason, we can explain the magnetic orders at $x \sim 0$ and 0.4, by assuming a simple monotonic x-dependence of the interaction: Here, we introduce $\bar{U}(x)$ by the liner interpolation between U_c for $x = 0$ and that for $x = 0.4$, as shown in Fig. 3 (a). The x-dependence of $\bar{U}(x)$ might be explained by the change in the d-electron Wannier functions [23], or the underestimation of the bandwidth given by the first-principle study for $x \sim 0.4$.

We also analyze the SC state using the linearized Eliashberg equation:

$$\lambda_{\rm E}\Delta_{ll'}(k) = -\frac{T}{N}\sum_{k',m_i} W_{lm_1,m_4l'}(k-k')G'_{m_1m_2}(k') \times \Delta_{m_2m_3}(k')G'_{m_4m_3}(-k') + \delta\Sigma^a_{ll'}(\epsilon_n), \quad (3)$$

where $\Delta_{ll'}(k)$ is the gap function, and $\lambda_{\rm E}$ is the eigenvalue that reaches unity at $T = T_{\rm c}$. When T is fixed, the larger value of $\lambda_{\rm E}$ would correspond to the higher $T_{\rm c}$. Here, $\hat{W}$ is the pairing interaction given by the RPA, $(\hat{G}')^{-1} = (\hat{G})^{-1} - \delta\hat{\Sigma}^n$ is the normal Green function with impurity-induced normal self-energy $\delta\hat{\Sigma}^n$, and $\delta\hat{\Sigma}^a$ is

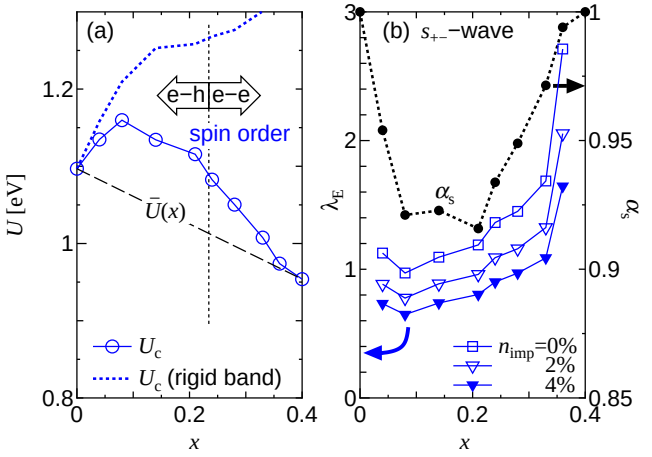

FIG. 3: (Color online) (a) U_c in present models (solid line) and that in the rigid band model (dotted line) against x for $g = 0$. $\bar{U}(x)$ is determined by liner interpolation between U_c for $x = 0$ and that for $x = 0.4$. (b) Obtained λ_E for the $s_{\pm}$-wave state with $n_{\rm imp} = 0\%, 2\%, 4\%$. The x-dependence of α_s is also shown.

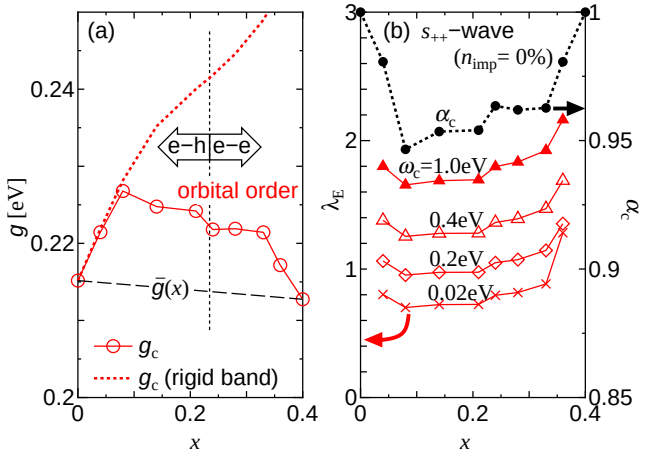

FIG. 4: (Color online) (a) g_c in present models (solid line) and that in the rigid band model (dotted line) against x for $U = 0$. $\bar{g}(x)$ is determined by liner interpolation between g_c for $x = 0$ and that for $x = 0.4$. (b) Obtained λ_E for the s_{++}-wave state with $\omega_c = 0.02 \sim 1$ ($n_{\rm imp} = 0$). The x-dependence of α_c is also shown.

the impurity-induced anomalous self-energy. The expressions are given in Ref. [10]. Hereafter, we put the orbital-diagonal on-site impurity potential as $I = 1$. Figure 3 (b) shows the obtained $\lambda_{\rm E}$ as a function of x. We see that $\lambda_{\rm E}$ has two peaks at both $x = 0.04$ and $x = 0.36$ since $\chi^s(\boldsymbol{Q})$ develops divergently toward $x \to 0$ and 0.4. Then, the double-dome behavior of $T_{\rm c}$ in $LaFeAsO_{1-x}H_x$ would be explained, since $T_{\rm c}$ at both boundaries will be suppressed by the magnetic and orbital orders. Here, the hole-pockets still exist even at $x = 0.4$, and then the e-e FS nesting $\boldsymbol{Q} \approx (\pi, \pi/3)$ contributes to the $s_{\pm}$-wave state. The d-wave state is expected if the hole-pockets disap-

pear [24–26], while the relation $\lambda_{\rm E}(s_{\pm}\text{-wave}) > \lambda_{\rm E}(d\text{-wave})$ is realized for $x < 0.4$ in the present study. In both states, $\lambda_{\rm E}$ is quickly suppressed when the impurity concentration $n_{\rm imp}$ is finite, meaning that the $s_{\pm}$- and d-wave states are fragile against impurities.

In the next stage, we study the development of the orbital susceptibility by g, by putting $U = 0$. Figure 4 (a) shows the x-dependence of g_c, given by the condition $\alpha_c = 1$. Similarly to Fig 3 (a), we introduce $\bar{g}(x)$ by liner interpolation between g_c for $x = 0$ and that for $x = 0.4$ in Fig. 4 (a). Then, the orbital ordered states are realized for both $x \sim 0$ and $x \sim 0.4$. The obtained $\chi^{\rm c}_{2424}(\boldsymbol{q})$ by the RPA for $x = 0.4$ is shown in Fig. 5 (a). We also study the orbital-fluctuation-mediated s_{++}-wave state for $g = \bar{g}(x)$: Figure 4 (b) shows the obtained $\lambda_{\rm E}$ as a function of x. The behavior of $\lambda_{\rm E}$ in the s_{++}-wave state is similar to that of the $s_{\pm}$-wave state because orbital susceptibilities develop divergently toward $x \to 0$ and 0.4. For this reason, the double-dome behavior of $T_{\rm c}$ can be also explained by the orbital fluctuations. The value of $\lambda_{\rm E}$ increases for larger cutoff energy ω_c: In Ref. [10], we put $\omega_c = 0.02$ since we considered the quadrupole interaction due to the Fe-ion oscillations. However, ω_c for the effective quadrupole interaction due to VC [12] depends on the electronic state and not unique. In both cases, we should use larger ω_c since the used temperature ($T = 0.02$) is much higher than the real $T_{\rm c}$.

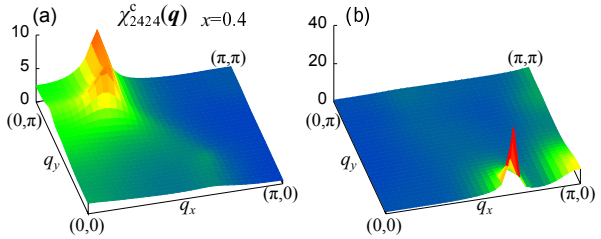

FIG. 5: (Color online) (a) $\chi^{\rm c}_{2424}(\boldsymbol{q})$ given by the RPA using the quadrupole interaction in Eq. (1) for $\alpha_c = 0.98$ (b) $\chi^{\rm c}_{2424}(\boldsymbol{q})$ given by the SC-VC method using the Hubbard interaction for $\alpha_c = \alpha_s = 0.98$.

Finally, we explain that the spin and orbital fluctuations mutually develop by taking the VC into account, as actually observed in various Fe-based superconductors [4, 14]. Beyond the RPA, $\hat{\chi}^0(q)$ in Eq. (2) is replaced with $\hat{\chi}^0(q) + \hat{X}^{\rm s(c)}(q)$, where $\hat{X}^{\rm s(c)}$ is the VC due to the Coulomb interaction for the spin (charge) channel. In the RPA, the VC is neglected irrespective of its importance. We developed the self-consistent VC (SC-VC) method in Ref .[12], and found that the Aslamazov-Larkin-type VC gives the large mode-coupling between spin and orbital, and the spin fluctuations induce strong orbital fluctuations due to this coupling. Figure 5 (b) shows the strong development of antiferro-orbital fluctuations, $\chi^{\rm c}_{2424}(\boldsymbol{q}) \gg 1$, given by the SC-VC method for $x = 0.4$, $U = 1.1$, $J/U = 0.073$ and $g = 0$. Therefore, the RPA analysis using $\bar{U}(x)$ and $\bar{g}(x)$ is justified by the SC-VC theory.

In addition, strong ferro-orbital fluctuations, that correspond to the orthorhombic structure transition, are also induced by the Aslamazov-Larkin-type VC for $x \sim 0$ [12, 27]. The orbital fluctuations due to VC also occur in a simple two-orbital model, which would explain the nematic order in $Sr_3Ru_2O_7$ [28, 29]. We have recently developed the SC-VCΣ method, in which both the self-energy and the VC are taken into account [30]. Using this method, the s_{++}-wave state can be realized for realistic parameters ($J/U \sim 0.1$) for $x \sim 0$ even for $g = 0$. It is an important future problem to analyze the present model using the SC-VCΣ method.

In summary, we have explained the reappearance of the spin and orbital orders in $LaFeAsO_{1-x}H_x$ at $x \sim 0$ and $x \sim 0.4$. Both spin and orbital orders originate from the commensurate e-h FS nesting for $x \sim 0$, and incommensurate e-e FS nesting for $x \sim 0.4$. Due to strong spin and orbital fluctuations at $x \sim 0$ and 0.4, both the spin-fluctuation mediated $s_{\pm}$-wave state and orbital-fluctuation mediated s_{++}-wave state can be realized, depending on the magnitude relation of these fluctuations. Since small impurity effect on $T_{\rm c}$ for the first SC dome [16, 17] indicates the s_{++}-wave state, the $s_{++} \to s_{\pm}$ crossover will occur with doping, in case that the second SC dome is the $s_{\pm}$-wave state [10]. Thus, the impurity effect study for $x \sim 0.4$ is highly required.

This study has been supported by Grants-in-Aid for Scientific Research from MEXT of Japan. The part of Tokyo Tech was supported by JSPS First Program. Numerical calculations were partially performed using the Yukawa Institute Computer Facility.

[1] Y. Kama, T. Watanabe, M. Hirano, and H. Hosono, J. Am. Chem. Soc. **130**, 3296 (2008).
[2] T. Shimojima, K. Ishizaka, Y. Ishida, N. Katayama, K. Ohgushi, T. Kiss, M. Okawa, T. Togashi, X.-Y. Wang, C.-T. Chen, S. Watanabe, R. Kadota, T. Oguchi, A. Chainani, and S. Shin, Phys. Rev. Lett. **104**, 057002 (2010).
[3] M. Yi, D. H. Lu, J.-H. Chu, J. G. Analytis, A. P. Sorini, A. F. Kemper, S.-K. Mo, R. G. Moore, M. Hashimoto, W. S. Lee, Z. Hussain, T. P. Devereaux, I. R. Fisher, Z.-X. Shen, PNAS **108**, 6878 (2011).
[4] M. Yoshizawa, R. Kamiya, R. Onodera, Y. Nakanishi, K. Kihou, H. Eisaki, and C. H. Lee, Phys. Soc. Jpn. **81**, 024604 (2012).
[5] T. Goto, R. Kurihara, K. Araki, K. Mitsumoto, M. Akatsu, Y. Nemoto, S. Tatematsu, and M. Sato, J. Phys. Soc. Jpn. **80**, 073702 (2011).
[6] K. Kuroki, S. Onari, R. Arita, H. Usui, Y. Tanaka, H. Kontani, and H. Aoki, Phys. Rev. Lett. **101**, 087004 (2008).

[7] I. I. Mazin, D.J. Singh, M.D. Johannes, and M.H. Du, Phys. Rev. Lett. **101**, 057003 (2008).

[8] S. Graser, G. R. Boyd, C. Cao, H.-P. Cheng, P. J. Hirschfeld, and D. J. Scalapino, Phys. Rev. B **77**, 180514(R) (2008).

[9] A. V. Chubukov, D. V. Efremov, and I. Eremin, Phys. Rev. B **78**, 134512 (2008).

[10] H. Kontani and S. Onari, Phys. Rev. Lett. **104**, 157001 (2010).

[11] H. Kontani, Y. Inoue, T. Saito, Y. Yamakawa and S. Onari, Solid State Communications, **152** (2012) 718.

[12] S. Onari and H. Kontani, Phys. Rev. Lett. **109**, 137001 (2012).

[13] S. Iimura, S. Matuishi, H. Sato, T. Hanna, Y. Muraba, S. W. Kim, J. E. Kim, M. Takata and H. Hosono, Nat. Commun., **3**, 943 (2012).

[14] N. Fujiwara *et al.,* unpublished.

[15] T. Nakano, N. Fujiwara, K. Tatsumi, H. Okada, H. Takahashi, Y. Kamihara, M. Hirano and H. Hosono, Phys. Rev. B **81**, 100510(R) (2010).

[16] M. Sato, Y. Kobayashi, S. C. Lee, H. Takahashi, E. Satomi, and Y. Miura, J. Phys. Soc. Jpn. **79**, 014710 (2009); S. C. Lee, E. Satomi, Y. Kobayashi, and M. Sato, J. Phys. Soc. Jpn. **79**, 023702 (2010).

[17] J. Li, Y. Guo, S. Zhang, S. Yu, Y. Tsujimoto, H. Kontani, K. Yamaura, and E. Takayama-Muromachi, Phys. Rev. B **84**, 020513(R) (2011).

[18] Y. Nakajima, T. Taen, Y. Tsuchiya, T. Tamegai, H. Kitamura, and T. Murakami, Phys. Rev. B **82**, 220504 (2010).

[19] J. Li, Y. Guo, S. Zhang, S. Yu, Y. Tsujimoto, H.Kontani, K. Yamaura, and E. Takayama-Muromachi: Phys. Rev. B **84**, 020513(R) (2011).

[20] S. Onari and H. Kontani, Phys. Rev. Lett. **103**, 177001 (2009).

[21] Y. Yamakawa, S. Onari, and H. Kontani, arXiv:1303.2978.

[22] J. Kunes, R. Arita, P. Wissgott, A. Toschu, H. Ikeda, and K. Held, Comput. Phys. Commun. **181**, 1888 (2010)

[23] T. Miyake, K. Nakamura, R. Arita and M. Imada, J. Phys. Soc. Jpn. **79**, 044705 (2010).

[24] F. Wang, F. Yang, M. Gao, Z.Y. Lu, T. Xiang, and D.H. Lee, Europhy. Lett. **93**, 57003 (2011).

[25] T.A. Maier, S. Graser, P.J. Hirschfeld, and D.J. Scalapino, Phys. Rev. B **83**, 100515(R) (2011).

[26] T. Saito, S. Onari, and H. Kontani, Phys. Rev. B **83**, 140512(R) (2011)

[27] H. Kontani, T. Saito and S. Onari, Phys. Rev. B **84**, 024528 (2011)

[28] Y. Ohno, M. Tsuchiizu, S. Onari, and Hiroshi Kontani, J. Phys. Soc. Jpn. **82**, 013707 (2013).

[29] M. Tsuchiizu, S. Onari, and H. Kontani, arXiv:1211.3944.

[30] S. Onari and H. Kontani, unpublished.